EUROPEAN ORGANIZATION FOR NUCLEAR RESEARCH

CERN-PPE/96-49
April 1, 1996

Measurement of the Branching Ratios $\mathbf{b \to e\,\nu X}$, $\boldsymbol{\mu\,\nu}\mathbf{X}$, $\boldsymbol{\tau\,\nu}\mathbf{X}$ and $\boldsymbol{\nu}\mathbf{X}$

The L3 Collaboration

Abstract

The inclusive semileptonic branching ratios b $\to$ e νX, μ νX, τ νX and νX have been measured at LEP with the L3 detector. The analysis is based on 2–jet hadronic Z decays obtained in the data collected between 1991 and 1992. Three separate event samples are analysed, containing electrons, muons and large missing energy (neutrinos), respectively. From the electron sample, we measure Br(b $\to$ e νX) = (10.89$\pm$0.20$\pm$0.51)% and, from the muon sample, Br(b $\to$ μ νX) = (10.82$\pm$0.15$\pm$0.59)%, where the first error is statistical and the second is systematic. From the missing energy sample, we measure Br(b $\to$ νX) = (23.08$\pm$0.77$\pm$1.24)%, assuming the relative semileptonic decay rates e:μ:τ = 1:1:(0.25$\pm$0.05), according to theoretical expectations. From a combined analysis of all three samples and constraining the relative semileptonic rates, we measure Br(b $\to$ eνX) = Br(b $\to$ $\mu\,\nu$X) = (10.68$\pm$0.11$\pm$0.46)%. Alternatively, we can remove the constraint on the relative semileptonic rates and measure Br(b $\to$ τ νX) = (1.7$\pm$0.5$\pm$1.1)%.

Submitted to *Zeitschrift für Physik C*

1 Introduction

A measurement of the semileptonic branching ratio Br(b$\rightarrow$ $\ell\nu$X), from hadronic Z decays, is described. Measurements of the semileptonic branching ratios are usually made with electrons and muons. However, they can also be measured with neutrinos, using the missing energy spectrum of b jets. The neutrino energy can be obtained indirectly using the difference between the kinematically constrained jet energy, assumed to be the beam energy, and the measured jet energy ($E_\nu \approx E_{beam} - E_{jet}$).

This measurement with energetic neutrinos is the first determination of Br(b$\rightarrow$ νX). The systematic errors due to backgrounds and efficiencies are different from the measurements with electrons and muons, and the result is thus complementary to the traditional measurements with inclusive electrons and muons. Furthermore, combined with the branching ratio obtained with inclusive electrons and muons, the result is sensitive to the polarization of the virtual W [1] and to the decay b$\rightarrow$ $\tau\nu$X.

The neutrino analysis is restricted to two–jet events since the method for determining the neutrino energy is not valid for three–jet events originating from hard gluon radiation. In order to compare the neutrino branching ratio measurement with the results obtained with electrons and muons, all measurements are done for the same sample of hadronic two–jet Z decays. This differs from previous measurements of the b semileptonic branching ratio with L3, which made no requirements on the event shape [2].

2 The L3 detector and the hadronic event selection

The data were collected with the L3 experiment at LEP between 1991 and 1992. During this period the L3 detector consisted of a central tracking chamber, a high resolution electromagnetic calorimeter composed of BGO crystals, a cylindrical array of scintillation counters, a uranium/brass hadron calorimeter with proportional wire chamber readout, and a precise muon spectrometer. These subdetectors are installed in a 12 m diameter solenoid which provides a uniform magnetic field of 0.5 T along the beam direction. A detailed description of the L3 detector can be found elsewhere [3]. The b lifetime tagging in this analysis is based on the measurement of charged tracks in the central tracking chamber. This device is a precision Time Expansion Chamber which consists of two coaxial cylindrical drift chambers. The inner chamber is divided into 12 sectors, each with 8 sense wires. The outer chamber has 24 sectors, each with 54 sense wires. Tracks are reconstructed with up to 62 wires signals at radii between 11 cm and 43 cm. For tracks that are not close to an anode or cathode plane, the single hit resolution varies between 50–60 μm, resulting in a momentum resolution of $\Delta p_t/p_t$ of $0.018\times p_t$ and an impact parameter resolution of 109 μm for isolated tracks. The two track separation is about 600 μm.

To reduce the amount of missing energy due to initial–state bremsstrahlung only the events taken within $\pm$0.5 GeV of the Z peak are used. This data sample corresponds to approximately 900k hadronic Z decays.

The hadronic events are selected with criteria similar to the ones used for the measurement of the total hadronic cross section in [4]. To reduce possible selection biases for events with large missing energy due to energetic neutrinos from b hadron decays, the requirements on the visible energy and the transverse energy imbalance of the events are relaxed and new criteria are introduced to reduce backgrounds from two–photon and $\tau^+\tau^-$ events to a negligible level. Since the branching ratio analysis for each channel is limited by systematic uncertainties, it is further required that the hadronic events are well contained in the hermetic barrel region of the detector. The following additional selection criteria are used:

- The visible energy in each hemisphere, defined by the thrust axis of the event, must be larger than 10% of the beam energy.
- The polar angle, θ_{jet}, of the momentum vector sum of all calorimeter clusters associated with each hemisphere (jet) has to fulfil the condition $|\cos\theta_{jet}| < 0.7$. For the branching ratio measurements only those jets that satisfy the condition $|\cos\theta_{jet}| < 0.65$ are analysed.
- The energy sum of all calorimeter clusters with $|\cos\theta_{cluster}| > 0.74$ must be smaller than 5 GeV.
- Two–photon background events are suppressed by requiring that the visible energy of the event is larger than 40% of the center–of–mass energy. Furthermore, for the events with a visible energy of less than 70% of the center–of–mass energy, the missing transverse energy of the event must be either larger than 50% of the beam energy or be larger than the missing longitudinal energy.
- The remaining $\tau^+\tau^-$ background is suppressed by requiring at least five charged tracks. In addition, one hemisphere must contain at least three tracks, each with a transverse momentum with respect to the beam of more than 150 MeV and a distance of closest approach with respect to the beam axis smaller than 1 mm.

A total of 402k hadronic events fulfil these criteria. A geometrical cone algorithm with a half angle of 20° is used to form jets from the calorimeter clusters, starting from the most energetic clusters. If more than one such jet is found in a hemisphere, these jets are combined into one jet, provided their invariant mass is smaller than 25 GeV. Using this jet definition, the events are divided into "two–jet" and "three–jet" events. Out of the selected hadronic events, 86.1% (346k) are classified as two–jet events.

Monte Carlo events are simulated using JETSET 7.3 with the parton shower approximation for gluon radiation and string fragmentation [5] and a GEANT–based description of the L3 experiment [6]. Weak decays of c and b hadrons are simulated such that the measured inclusive charged lepton spectra and the branching ratios for charm and beauty decays [7] are reproduced. The simulated energy spectra of electrons, muons and neutrinos, with an inclusive $\mathrm{Br}(\mathrm{b}\to \ell\nu \mathrm{X})$ of 10.45%, agree also with the inclusive lepton spectra obtained for b hadron decays from the ACCMM model [8]. More details about the simulation of weak decays of c and b hadrons are given in [9].

The energy spectra of the primary b hadrons are simulated with the Peterson function [10] as implemented in JETSET, adjusted such that the average energy of the weakly decaying b hadrons ($\mathrm{B_d}$, $\mathrm{B_u}$, $\mathrm{B_s}$ and Λ_b) corresponds to $0.72\times E_{beam}$. With this simulation good agreement between the data and the Monte Carlo is obtained for the electron, the muon and the simultaneously measured neutrino energy spectra [9]. Using the same analysis chain as for the data, 497k fully simulated Monte Carlo events remain after the barrel event selection, out of which 85.3% (424k) events are classified as two–jet events. The fraction of b events in the two–jet sample is found to increase to 22.8%, to be compared with 21.6% in the full Monte Carlo sample.

2.1 Selection of b enriched and b depleted event subsamples

For the analysis four different event subsamples (I–IV) with enhanced or depleted b event fractions, as given in Table 1, are selected. These subsamples are used to control and correct the Monte Carlo signal efficiency and background estimates for the inclusive electron and muon analysis. Subsample I, the lifetime tagged b events, is also used to measure the inclusive neutrino rate from the decay b$\rightarrow \nu$X.

Subsample	selection method	b purity	number of jets
I	lifetime tag	61%	79k
II	anti–lifetime tag	11%	177k
III	high x tag	10%	33k
IV	high $p_{\perp}$ lepton tag	83%	15k

Table 1: The different event subsamples used in the analysis to control signals and backgrounds. For subsamples I and II both event hemispheres are used while subsample III and IV are made from hemisphere tags and only the unbiased jet is used.

The lifetime based selection of b enriched and depleted event subsamples proceeds as follows. The events are separated into two hemispheres defined by the thrust axis of the event which is measured from the reconstructed calorimeter clusters. A secondary vertex for each hemisphere is obtained using well measured tracks. Events which have a large distance between the two reconstructed vertices are selected as candidates for b events.

For this distance determination only well measured tracks which fulfil the following conditions are used:

- The measured transverse momentum of each track with respect to the beam direction is required to be larger than 0.5 GeV.
- To ensure a good track measurement the first reconstructed hit has to be found in the inner tracking chamber. Furthermore, the reconstructed azimuthal track angle with respect to the anode or cathode wire planes is required to be larger than 15 mrad. For regions where the inner anode wire plane matches the outer cathode plane, this angle is required to be larger than 30 mrad.
- Secondary tracks from γ conversions, hadronic interactions, as well as those from K and Λ decays are suppressed by requiring that the distance of closest approach with respect

to the average primary hadronic vertex, determined for each LEP fill ("fill vertex"), is smaller than 1.2 mm.

- To obtain a good accuracy for the vertex determination, the angle of a track with respect to the thrust axis is required to be larger than 75 mrad.

The accepted tracks are used to determine a secondary vertex with the b hadron flight direction approximated by the thrust axis of the event. The average value of these track vertices per hemisphere is used, weighting each track with the measured $p_\perp$ with respect to the thrust axis. If more than three tracks are accepted per hemisphere, the three tracks with the largest distances with respect to the fill vertex are used to estimate the secondary vertex separately for each hemisphere. This secondary vertex distance is assumed to be zero if no track is accepted. The best sensitivity to b events is obtained using the distance between the two reconstructed hemisphere vertices. The distance distributions for the data and the Monte Carlo are shown in Figure 1. The distance distribution from Monte Carlo b events is also shown.

Events which have a distance between the two vertices of more than 3.5 mm define the b enriched subsample I. Events with a reconstructed negative decay distance between the two hemispheres are used to define subsample II.

The light quark enriched event subsample III is selected with the requirement that a high $x(= E/E_{beam})$ particle is found in at least one jet. It is required that either a high momentum track with a momentum above 60% of the beam energy and an associated calorimeter cluster of more than 50% of the beam energy, or an energetic π^0 candidate with an energy above 50% of the beam energy is found in one jet. The jet in the opposite hemisphere defines this light quark enriched jet sample. Due to the hard fragmentation function of c and b hadrons, and their subsequent decays, it is very rare to find a particle with high x in c and b events. This method to enrich light quark events was first used in 1985 by HRS [11].

Finally the b enriched jet subsample (IV) is selected from jets that are opposite to those containing a high p and $p_\perp$ electron or muon candidate, as defined in sections 2.2 and 2.3.

2.2 Selection of inclusive electron events

Electron candidates are selected with the following criteria:

- The energy of a cluster, E_{BGO}, in the barrel BGO calorimeter (with a polar angle θ satisfying $|\cos\theta| < 0.72$) must be larger than 3 GeV. The hadronic calorimeter energy associated with this cluster must be smaller than 2 GeV.

- Between 10 and 40 crystals are associated with the BGO cluster and more than 95% of the energy is deposited in the central 9 crystals.

- One charged track must point to this BGO cluster and the difference between the azimuthal angle estimated from the shower center and the estimated track impact point at the BGO calorimeter must be smaller than (4 mrad + 8 mrad/E_{BGO} [GeV]). To suppress background from photon conversions it is required that no other track is pointing within 5 mrad to this cluster.

- The measured p_t with respect to the beam direction for the charged track must be consistent with the E_t measurement from the BGO calorimeter ($|1/E_t - 1/p_t| < 0.05$ GeV^{-1}).

With these criteria, 8.2k electron candidates are selected in the two–jet event sample. Out of these, 5.3k electron candidates have a $p_\perp$ with respect to the jet direction of more than 1.4 GeV.

2.3 Selection of inclusive muon events

Muon candidates are selected using the following criteria:

- Tracks found in the barrel muon system must be reconstructed in at least two out of the three ϕ–layers and one out of the two possible Z–chamber layers.
- The track momentum, measured from the muon chambers and corrected for the energy loss in the calorimeter, must be larger than 4 GeV.
- The distance of closest approach to the fill vertex in the transverse plane, extrapolated taking into account the errors due to multiple scattering, must be smaller than 100 mm. This distance must also be smaller than three times the estimated distance error due to multiple scattering in the calorimeters.

With these criteria, 24.2k muon candidates are selected in the two–jet event sample. Out of these 9.8k have a $p_\perp$ of more than 1.4 GeV with respect to the jet direction. The efficiency and background for the muon sample are both larger than those for the electron sample. The main reason is that the muon identification imposes no isolation criteria. For the inclusive electron selection, the required electromagnetic shower shape of the cluster essentially selects isolated electrons.

2.4 Inclusive neutrinos in jets with low visible energy

The visible energy distribution for b jets in the Monte Carlo is shown in Figure 2a. Jets associated with semileptonic b decays dominate the region of jets with low visible energy (large missing energy). For example, about 82% of b jets with a visible energy of less than 30 GeV (a missing energy of more than 15 GeV) originate from semileptonic b decays. The backgrounds in the data are from mismeasured jets and semileptonic c decays. The visible energy spectrum of jets containing semileptonic b decays from the Monte Carlo is shown in Figure 2b. The contributions from the generated decays b$\rightarrow$ eνX, b$\rightarrow$ $\mu\nu$X and b$\rightarrow$ $\tau\nu$X, including the subsequent c hadron and τ decays, are shown separately. The visible energy spectra of jets associated with the decays b$\rightarrow$ eνX and b$\rightarrow$ $\mu\nu$X are slightly different. Since undetected muons increase the missing energy, while the energy from unidentified electrons is still measured in the calorimeter.

The energy measurement for jets with large missing energy due to mismeasured jets is compared in the data and Monte Carlo using the b depleted subsamples (II and III) and are shown in Figures 3a and b respectively. While the mean jet energy values are well described, the jet energy resolution ($\sigma \approx 4.2$ GeV) is about 10% smaller in the data than in the Monte Carlo. The Monte Carlo also underestimates the number of jets with large missing energy by roughly 15%. Therefore, the data will be used to determine the background, as described in section 4. More details about the jet energy measurement are given in reference [9].

In order to use the missing energy signature of jets to measure Br(b$\rightarrow$ νX), backgrounds from mismeasured jets must be reduced as much as possible. Therefore the b enriched event subsample I is used for this measurement. With the requirement that the measured polar angle of the jet fulfils the condition $|\cos\theta_{jet}| < 0.65$, about 79k jets are analyzed.

3 Measurement of Br(b$\rightarrow \ell\nu X$)

The inclusive Br(b$\rightarrow$ $\ell\nu$X) values for electrons, muons and neutrinos are obtained from a comparison of the observed number of inclusive electrons, muons and jets with large missing energy in the data and the Monte Carlo with respect to the number of b jets. Lepton detection efficiencies and backgrounds have been estimated using data and Monte Carlo. The different branching ratios are estimated with respect to the number of b jets, obtained from the Monte Carlo simulation with the Standard Model value for R_b of 0.216. If the recent experimental value of 0.2209 ± 0.0021 is used for R_b [12], all semileptonic branching ratios would decrease by (2 ± 1)% of their measured value.

The fraction of semileptonic b decays is enhanced using a high value for the $p_\perp$ of the electrons and muons with respect to the jet direction. The jet direction is determined from all calorimeter clusters in a hemisphere except the one of the lepton candidate.

The semileptonic branching ratios are measured with the two–jet event sample and requiring electron and muon candidates with high $p_\perp$ (>1.4 GeV) with respect to the closest jet. For an estimate of the systematic error due to the event selection, the $p_\perp$ and the two–jet event definitions are varied. Using a different charged lepton spectrum in the b hadron rest frame for the efficiency determination, as for example obtained with the ISGW model [13], relative branching ratio changes of about 3–4% have been found previously at the $\Upsilon(4S)$ resonance [14]. In Z decays the lepton p and $p_\perp$ spectra depend also on the boost of the b–hadron. Having the constraint from the observed lepton momentum spectrum, we find that the assumptions of the b decay model and the b fragmentation are strongly correlated. For example, a softer lepton spectrum in the b rest frame would thus have to be compensated by a slightly harder b fragmentation function. The size of the related systematic errors is estimated from the stability of the branching ratio as a function of the charged lepton p and $p_\perp$.

For the analysis related to the missing energy spectrum of b jets, the neutrino energy spectrum is obtained from the free b quark decay model with a V–A decay spectrum. The branching ratio uncertainties related to the used b decay model have been estimated from the results of our previous measurement of the neutrino energy spectrum in identified semileptonic b decays [9]. In this measurement we have achieved an energy scale uncertainty of better than $\pm$ 200 MeV. This energy uncertainty, used for the error estimate of the branching ratio, was found to be much larger than uncertainties due to the choice of the b–decay model where typical differences are in the range of 50–80 MeV.

3.1 Br(b$\rightarrow$eνX) measurement

The $p_\perp$ spectrum for electron candidates with a momentum above 3 GeV is shown in Figure 4a for the data and the Monte Carlo, normalized to the number of selected hadronic events. For low $p_\perp$ values about 30% more electron candidates are found in the data than in the Monte Carlo. There is a smaller excess seen in the b enriched subsample I (Figure 4b), while an even larger excess of low $p_\perp$ electron candidates is found in the b depleted event subsample II (Figure 4c) and subsample III. Therefore, it can be concluded that the Monte Carlo underestimates the electron background in the low $p_\perp$ regions. For $p_\perp$ values of less than 0.7 GeV, where a significant difference between the data and the Monte Carlo is observed, a correction for the Monte Carlo background estimate is applied by assuming that the background is underestimated by the excess observed in the low $p_\perp$ region of the b depleted event subsamples II and III.

For larger $p_\perp$ values of the electron candidates one finds good agreement between the data and the Monte Carlo for the different subsamples. The fraction of electron candidates per hadronic event in the data and the Monte Carlo for different $p_\perp$ values, and the resulting branching ratios, are given in Table 2.

The momentum spectra for the electron candidates with a $p_\perp$ between 1.4 GeV and 2.1 GeV and above 2.1 GeV are shown in Figures 5a and b, respectively. While the overall shape of the momentum spectrum is well described by the Monte Carlo, there is a discrepancy for low momentum electron candidates with $p_\perp$ larger than 2.1 GeV. Using only the electron candidates with momenta above 6 GeV, the result given below decreases by about 0.1%.

	Data	Monte Carlo		Data
$p_\perp$ [GeV]	$n_{e^\pm}/n_{had} \times 10^3$	$n_{e^\pm}/n_{had} \times 10^3$	purity b$\rightarrow$ eνX [%]	Br[%]
0.0–0.7	2.09$\pm$0.08	1.54$\pm$0.06	28.5	9.55$\pm$1.28
0.7–1.4	6.14$\pm$0.13	5.98$\pm$0.12	48.3	11.01$\pm$0.32
1.4–2.1	6.11$\pm$0.13	6.04$\pm$0.12	73.3	10.61$\pm$0.31
>2.1	9.32$\pm$0.16	8.92$\pm$0.15	78.3	11.05$\pm$0.27
> 1.4	15.43$\pm$0.21	14.96$\pm$0.19	76.3	10.89$\pm$0.20

Table 2: The observed number of electron candidates per hadronic event in the data and in the Monte Carlo and the resulting Br(b$\rightarrow$ eνX) with the statistical errors are given for different $p_\perp$ values. A $p_\perp$ cut of 1.4 GeV is used to extract the final semileptonic branching ratio. For the Monte Carlo, with an input branching ratio of 10.45%, the purity of correctly identified semileptonic b decays is also given.

Adding all the systematic errors in quadrature, as discussed in detail in section 3.3, the Br(b→ $e\nu X$) measured with inclusive electron candidates and a $p_\perp$ of more than 1.4 GeV is (10.89±0.20±0.51)%.

3.2 Br(b→$\mu\nu X$) measurement

The $p_\perp$ spectrum with respect to the jet for the inclusive muon candidates with a momentum above 4 GeV is shown in Figure 6a for the data and the Monte Carlo, normalized to the number of selected hadronic events. The $p_\perp$ spectrum of the inclusive muon candidates is well described by the Monte Carlo. Furthermore, good agreement between the data and the Monte Carlo is also found for the $p_\perp$ spectra in the b enriched and b depleted event subsamples I–IV. For example, the $p_\perp$ spectrum for the muon candidates in subsamples I and II are shown in Figure 6b and c respectively. One concludes that the backgrounds are accurately described by the Monte Carlo. The momentum spectra of the muon candidates with a $p_\perp$ between 1.4 and 2.1 GeV and more than 2.1 GeV are shown in Figures 7a and b, respectively. Again, as has been seen with the inclusive electron analysis, the low momentum range for muon candidates with $p_\perp$ larger than 2.1 GeV is not well described. As in the electron case, the result given below decreases by about 0.1% if only the muon candidates with momenta above 6 GeV are used.

The fraction of muon candidates per hadronic event found in the data and in the Monte Carlo for different $p_\perp$ bins and for different event subsamples are given in Table 3. Adding

	Data	Monte Carlo		Data
$p_\perp$ [GeV]	$n_{\mu^\pm}/n_{had} \times 10^3$	$n_{\mu^\pm}/n_{had} \times 10^3$	purity b→ $\mu^\pm\nu$X [%]	Br[%]
0.0–0.7	21.09±0.25	21.36±0.22	9.2	9.88±0.42
0.7–1.4	20.47±0.24	20.99±0.22	29.3	9.57±0.15
1.4–2.1	12.46±0.19	12.41±0.17	61.8	10.51±0.22
> 2.1	15.90±0.21	15.29±0.19	71.2	11.03±0.20
>1.4	28.36±0.29	27.71±0.26	67.0	10.82±0.15

Table 3: The observed number of muon candidates per hadronic event in the data and in the Monte Carlo. The resulting semileptonic branching ratio Br(b→ $\mu\nu$X) with the statistical errors are given for different $p_\perp$ values. A $p_\perp$ cut of 1.4 GeV is used to extract the final semileptonic branching ratio. For the Monte Carlo with an input semileptonic branching ratio of 10.45%, the purity of correctly identified semileptonic b decays is also given.

all the systematic errors in quadrature, as discussed in section 3.3, the Br(b→ $\mu\nu$X) measured with the inclusive muon candidates with a $p_\perp$ of more than 1.4 GeV is (10.82±0.15±0.59)%.

3.3 Systematic errors and comparison with previous measurements

The systematic errors for the branching ratio measurements with inclusive electrons and muons have been estimated from the different sources listed in Table 4.

Efficiency uncertainties due to the detector simulation and the geometrical acceptance have been studied using variations of the different selection criteria as well as the angular distributions of the electrons and muons in the data and Monte Carlo. As a result of these studies the inefficiency of the muon chamber system for the data with respect to the Monte Carlo description has been estimated to be (5±2)% for the 1992 data and (3±1)% for the 1991 data. These estimates agree with independent studies performed with $\mu^+\mu^-$ pairs. The differences in the branching ratio for $p_\perp$ values between 1.4 and 2.1 GeV and for larger $p_\perp$ values with respect to the average, see tables 2 and 3, are used to estimate background and signal efficiency uncertainties. Uncertainties from c hadron decays have been estimated from a relative variation of ±10% for the semileptonic c hadron decay branching ratios.

The branching ratio uncertainties related to the assumed b hadron energy spectrum are estimated using the average momenta of the inclusive electron and muon sample with a $p_\perp$ of more than 1.4 GeV in the data and in the Monte Carlo. It is found that the average momenta of the inclusive leptons in the Monte Carlo depend strongly on the average energy of the weakly decaying b hadrons and show a much smaller sensitivity to the semileptonic branching ratio. For example, the average electron or muon momenta increase by 80±20 MeV if the average energy of the weakly decaying b hadrons is increased by 450 MeV. A 10% relative increase of the branching ratio would change the average momenta by only −20±10 MeV for the inclusive electrons and by +40±10 MeV for the inclusive muons. The average momenta in the data are 180±110 MeV lower for the electron sample and 180±80 MeV higher for muons than the corresponding ones from the Monte Carlo, using an average energy of $x_E = 0.72$ for the weakly decaying b hadrons. The central value, $x_E = 0.72 \pm 0.02$, which we apply, provides the best description for the measured average momenta of the inclusive electron and muon candidates. This average energy value for the weakly decaying b hadrons is somewhat larger than the value $x_E = 0.70 \pm 0.02$, obtained from multiparameter fits to the inclusive lepton p and $p_\perp$ spectra [12]. The systematic error ±0.02 is derived from the difference between the best description of the electron spectrum (lower bound) and the best description of the muon spectrum (upper bound) and found to be consistent with an average value of $x_E = 0.70$. For a value of $x_E = 0.70$, the semileptonic branching ratio values would increase by 0.25% in absolute value and result in a poorer description of the measured lepton energy spectra.

	Branching Ratio systematic error [%]	
Error Source	b→ eνX	b→ $\mu\nu$X
selection efficiency	0.13	0.20
background and $p_\perp$ criteria	0.28	0.31
semileptonic c hadron decays	0.13	0.26
b hadron E spectrum ($< x_E >= 0.72 \pm 0.02$)	0.25	0.25
two–jet event selection	0.29	0.28
Combined Error	0.51	0.59

Table 4: Estimated contributions to the systematic error for the Br(b→ eνX) and Br(b→ $\mu\nu$X) using the high $p_\perp$ lepton selection.

The results obtained with inclusive electrons and muons are consistent and can be combined, giving an average Br(b→ e(μ)νX) value of (10.85±0.12±0.47)%. This result for the semileptonic branching ratio is about 1% lower than our previous result for the semileptonic branching ratio of (11.9±0.3±0.6)%, which was obtained using inclusive electrons and muons [2] in the 1990 data sample.

The origin of this difference has been investigated and the following two main sources have been identified, in addition to possible statistical fluctuations.

For this analysis the b hadron fragmentation function is harder. The average x_E value of weakly decaying b hadrons has been increased from 0.68±0.02 to 0.72±0.02. This energy increase is required in order to match simultaneously the measured average momenta of the charged leptons and neutrinos and accounts for a difference of about 0.5% in the branching ratio.

For this analysis, two–jet events are used, while the whole hadronic event sample was used for our previous measurement. Using the entire two and three–jet event sample to determine the branching ratio with the current analysis, branching ratios of (11.0±0.2)% and (11.1±0.2)% are obtained with inclusive electron and muon candidates respectively. However, in contrast to the good agreement between data and the Monte Carlo for the lepton p and $p_\perp$ spectra in the two–jet event sample, discrepancies between the spectra are seen for the entire event sample. This is related to the simulation of b events in the three–jet sample as disagreements between data and Monte Carlo are also seen for the lifetime tagged b enriched and b depleted event subsamples, differently for the different flavour content. We have used the information from the lifetime tagged event samples to estimate corrections for the Monte Carlo efficiencies and backgrounds. With these corrections semileptonic branching ratios of (10.6±0.2)% and (10.8±0.2)% are determined with electrons and muons respectively in the entire event sample. Furthermore with these corrections the lepton p and $p_\perp$ spectra in the data and in the Monte Carlo are in reasonable agreement. In view of this discrepancy between data and Monte Carlo, the differences between the central value from the two–jet analysis and the uncorrected or corrected analysis for the entire event sample are used to estimate the uncertainty related to the branching ratio determination in the two–jet sample. The additional uncertainties for the branching ratio related to this discrepancy between data and Monte Carlo are ±0.29% for the measurement with electrons and ±0.28% for muons.

4 Br(b→νX) and Br(b→$\tau\nu$X) measurements

For the measurement of Br(b→ νX) the missing–energy spectrum of the jets in the lifetime tagged events, subsample I, is used. The efficiencies for tagging b events and light quark events from the Monte Carlo are corrected such that the obtained R_b value agrees with the Standard Model value of 0.216. For the correction of the tagging of b events the lifetime tagged events which contain in addition a high $p_\perp$ electron or muon candidates are used. The Monte Carlo efficiency to tag b events is corrected such that the semileptonic branching ratio in the lifetime tagged events which contain a high $p_\perp$ electron or muon candidate agrees with our directly measured semileptonic branching ratios using inclusive electron and muon candidates. With these constraints, the purity of b events in subsample I is found to be (59.4 ± 1.5)% in the data, 1.4% smaller than in the Monte Carlo simulation. The estimated uncertainty in the purity comes mainly from the statistical error obtained with the lifetime tagged high p and $p_\perp$ electron and muon candidates.

The missing energy spectrum of jets is used to extract either Br(b$\rightarrow \nu$X) or Br(b$\rightarrow \tau\nu$X). The neutrino energy spectrum for each type of semileptonic b decay is obtained from the Monte Carlo simulation with a (V–A)$\times$(V–A) b hadron decay structure. For the Br(b$\rightarrow \nu$X) measurement the neutrino spectrum is a combination of the different semileptonic b hadron decays, assuming that the b decay rate for the charged leptons (e:μ:τ) is 1:1:(0.25$\pm$0.05), where the error reflects the range of theoretical estimates [15]. Alternatively, the value Br(b$\rightarrow$ e(μ)νX) is constrained and the excess is associated with the decay b$\rightarrow \tau\nu$X.

To reduce the dependence on the Monte Carlo, the background in the missing–energy spectrum due to measurement errors is determined from the data itself. This background is from jets with purely hadronic b decays and from the remaining background from light quark jets. The background determination uses the constraint that the jet energy spectra of the two–jet event sample with a b purity of 22.8% and the lifetime tagged b enriched events, subsample I, have to be described simultaneously with the same inclusive branching ratio for b$\rightarrow \nu$X.

This method of estimating the background has been developed and tested with the Monte Carlo. It is found that this method allows an accurate background estimation from mismeasured jets over the entire visible jet energy spectrum and for different assumed semileptonic b decay branching ratios and b purities. For a known purity of the selected event samples, the Monte Carlo input branching ratio Br(b$\rightarrow \nu$X) can be determined with a systematic accuracy of better than $\pm$0.7%.

Using a maximum likelihood fit to describe the jet energy spectra of the two–jet sample and the subsample I, we obtain Br(b$\rightarrow \nu$X) of (23.08$\pm$0.77$\pm$1.24)%. The jet energy spectrum from subsample I and the result of the fit are shown in Figure 8.

The systematic errors for this result are summarized in Table 5 and have been found by varying the central values by one standard deviation. The uncertainty of the neutrino energy scale, $\pm$200 MeV, and the resulting neutrino energy spectra have been estimated from our recent measurement of the average neutrino energy [9]. This error includes the uncertainties due to the b fragmentation function and the modeling of semileptonic c decays.

To compare the Br(b$\rightarrow \nu$X) result obtained from neutrinos with the ones from electrons and muons, Br(b$\rightarrow \nu$X) has to be divided by 2.25. The result for Br(b$\rightarrow$ e(μ)νX) obtained from the neutrino measurement is $(10.26 \pm 0.34 \pm 0.55)$%. This result has comparable errors to the direct measurement using electrons and muons. The agreement with the direct semileptonic Br(b$\rightarrow \ell\nu$X) results obtained with electrons and muons indicates a consistent treatment of the energy spectra of the charged leptons and the corresponding neutrinos. For example, as a result of a V+A b decay structure, the neutrino would have a harder energy spectrum with an average energy increase of about 1.5 GeV. Consequently, since the efficiency is estimated with a soft neutrino spectrum according to a V–A b decay structure, an apparently higher branching ratio would be seen. From a Monte Carlo simulation of a V+A b decay structure, analysed with the neutrino spectrum from a V–A b decay simulation an apparent branching ratio of (27 ± 1)% is obtained. The data are thus inconsistent with a V+A b decay structure. This result confirms our previous measurement of the neutrino energy spectrum in b decays [9] and provides thus further evidence for parity violation due to the V–A structure in b decays.

If one uses the directly measured semileptonic Br(b$\rightarrow \ell\nu$X) with electrons and muons, one can alternatively determine the additional contribution to the missing energy spectrum from the decay b$\rightarrow$ $\tau\nu$X. Using the same method as above to determine the background and the directly measured branching ratios with electrons and muons the result for the Br(b$\rightarrow$ $\tau\nu$X) is $(1.7 \pm 0.5 \pm 1.1)\%$. The jet energy spectrum and the fit result are shown in Figure 9.

The systematic errors of this result, summarized in Table 5, come from the error on the semileptonic branching ratio measurement with electrons and muons, the error of the background estimation, the neutrino energy scale uncertainty and the b purity of the lifetime subsample I.

The comparison of our new result with different theoretical estimates for the ratio Br(b$\rightarrow$ $\tau\nu$X)/Br(b$\rightarrow$ eνX) [15] is shown in Figure 10 and found to be in good agreement with the predictions.

The result is also in agreement with other measurements of the semileptonic branching ratio Br(b$\rightarrow$ $\tau\nu$X) [16, 17]. With respect to our previous result [17], the measurement reported here is effectively made with a statistically independent sample, since it uses different tagging technique and different acceptance. The systematic error due to the semileptonic branching ratio Br(b $\rightarrow$ e(μ)νX), $\pm 0.79\%$ in this measurement, is fully correlated. Other correlated systematic errors combine to a total of only 0.3%, since the measurement presented here uses a different jet energy calibration [9] and a different analysis procedures.

	Branching Ratio systematic error [%]	
Error Source	b$\rightarrow$ νX	b$\rightarrow$ $\tau\nu$X
purity uncertainty of lifetime subsample	0.90	0.53
background uncertainties	0.61	0.33
neutrino energy scale error ($\pm$200 MeV)	0.56	0.43
ratio of e : μ : τ	0.20	—
Br(b$\rightarrow$ e(μ)X) uncertainty	—	0.79
Combined Error	1.24	1.10

Table 5: Estimated contributions to the systematic error for Br(b$\rightarrow$ νX) and Br(b$\rightarrow$ $\tau\nu$X) using the missing energy spectrum.

5 Summary

The semileptonic branching ratios Br(b$\rightarrow$ eνX) and Br(b$\rightarrow$ $\mu\nu$X) have been measured using inclusive electrons, muons and neutrinos from a two–jet hadronic event sample. The efficiency corrections for the measurement have been obtained from a JETSET simulation of b jets and lepton energy spectra from the ACCMM model with a polarization of the virtual W according to a V–A structure for b hadron decays. The efficiency and backgrounds obtained from the simulation have been controlled with b enriched and b depleted event subsamples. The results obtained for the semileptonic branching ratios are:

$$\mathrm{Br}(\mathrm{b}\rightarrow \mathrm{e}\nu\mathrm{X})=(10.89\pm0.20\pm0.51)\%,$$

$$\mathrm{Br}(\mathrm{b}\rightarrow \mu\nu\mathrm{X})=(10.82\pm0.15\pm0.59)\%.$$

The two measurements are consistent and can be combined, giving an average value of

$$\mathrm{Br}(\mathrm{b}\rightarrow \mathrm{e}\nu\mathrm{X})=\mathrm{Br}(\mathrm{b}\rightarrow \mu\nu\mathrm{X})=(10.85\pm0.12\pm0.47)\%$$

Using the measurement of the missing energy spectrum in lifetime tagged b enriched events, and assuming a b decay rate to charged leptons (e:μ:τ) of 1:1:(0.25±0.05), we obtain:

$$\mathrm{Br}(\mathrm{b}\rightarrow \nu\mathrm{X}) = (23.08\pm0.77\pm1.24)\%.$$

Combining these three measurements and taking correlations into account, we obtain:

$$\mathrm{Br}(\mathrm{b}\rightarrow \mathrm{e}\nu\mathrm{X})=\mathrm{Br}(\mathrm{b}\rightarrow \mu\nu\mathrm{X}) = (10.68\pm0.11\pm0.46)\%$$

This result is consistent with the values obtained by other LEP experiments[18] and the measurements from ARGUS and CLEO[19].

Using our direct measurements for Br(b→ e(μ)νX)=10.85% with electrons and muons we obtain

$$\mathrm{Br}(\mathrm{b}\rightarrow \tau\nu\mathrm{X}) = (1.7\pm0.5\pm1.1)\% \text{ and}$$

$$\mathrm{Br}(\mathrm{b}\rightarrow \tau\nu\mathrm{X})/\mathrm{BR}(\mathrm{b}\rightarrow \mathrm{e}\nu\mathrm{X}) =0.15\pm0.04\pm0.07.$$

Acknowledgements

We wish to express our gratitude to the CERN accelerator divisions for the excellent performance of the LEP machine. We acknowledge the contributions of all the engineers and technicians who participated in the construction and maintenance of this experiment.

References

[1] M. Dittmar and Z. Was, Phys. Lett. **B332** (1994) 168.

[2] L3 Collaboration, B. Adeva *et al.*, Phys. Lett. **B261** (1991) 177.

[3] L3 Collaboration, B. Adeva et al., Nucl. Inst. and Meth. **A289** (1990) 35 and
L3 Collaboration, O. Adriani *et al.*, Phys. Rep. **236** (1993) 1.

[4] L3 Collaboration, B. Adeva *et al.*, Z. Phys. **C51** (1991) 179.

[5] T. Sjöstrand, Comput. Phys. Commun. **39** (1986) 347;
T. Sjöstrand and M. Bengtsson, Comput. Phys. Commun. **43** (1987) 367;

[6] The L3 detector simulation is based on GEANT Version 3.14; see R. Brun *et al.*, GEANT 3, CERN DD/EE/84-1 (Revised), September 1987 and the GHEISHA program (H. Fesefeld, RWTH Aachen Report PITHA85/02 (1985) for the simulation of hadronic interactions.

[7] Particle Data Group, L. Montanet *et al.*, Phys. Rev. **D50** (1994) 1173;
DELCO Collaboration, W. Bacino *et al.*, Phys. Rev. Lett. **43** (1979) 1073;
MARK III Collaboration, R. M. Baltrusaitis *et al.*, Phys. Rev. Lett. **54** (1985) 1976.

[8] G. Altarelli *et al.*, Nucl. Phys. **B208** (1982) 365.

[9] L3 Collaboration, M. Acciarri et al., Phys. Lett. **B351** (1995) 375.

[10] C. Peterson *et al.*, Phys. Rev. **D27** (1983) 105.

[11] HRS Collaboration, P. Keston *et al.*, Phys. Lett. **B161** (1985) 412.

[12] The LEP Collaborations, CERN-PPE/96-017, submitted to NIM.

[13] N. Isgur *et al.*, Phys. Rev. **D39** (1989) 799.

[14] See, for example, R. H. Schindler page 1602 in the Particle Data Group, L. Montanet *et al.*, Phys. Rev. **D50** (1994).

[15] P. Heiliger and L. M. Sehgal, Phys. Lett. **B229** (1989) 409;
A. Falk *et al.*, Phys. Lett. **B326** (1994) 145.

[16] ALEPH Collaboration, D. Buskulic *et al.*, Phys. Lett. **B343** (1995) 444.

[17] L3 Collaboration, M. Acciarri *et al.*, Phys. Lett. **B332** (1994) 201.

[18] ALEPH Collaboration, D. Buskulic *et al.*, Z. Phys. **C62** (1994) 179;
DELPHI Collaboration, P. Abreu *et al.*, Z. Phys. **C66** (1995) 323;
OPAL Collaboration, R. Akers *et al.*, Z. Phys. **C60** (1993) 199.

[19] ARGUS Collaboration, H. Albrecht *et al.*, Phys. Lett. **B318** (93) 397;
CLEO Collaboration, B. Barish *et al* Phys. Rev. Lett. **76** (1996) 1570.

The L3 Collaboration:

M.Acciarri,[28] A.Adam,[47] O.Adriani,[17] M.Aguilar-Benitez,[27] S.Ahlen,[11] B.Alpat,[35] J.Alcaraz,[27] G.Alemanni,[23] J.Allaby,[18] A.Aloisio,[30] G.Alverson,[12] M.G.Alviggi,[30] G.Ambrosi,[20] H.Anderhub,[50] V.P.Andreev,[39] T.Angelescu,[13] D.Antreasyan,[9] A.Arefiev,[29] T.Azemoon,[3] T.Aziz,[10] P.Bagnaia,[38] L.Baksay,[45] R.C.Ball,[3] S.Banerjee,[10] K.Banicz,[47] R.Barillère,[18] L.Barone,[38] P.Bartalini,[35] A.Baschirotto,[28] M.Basile,[9] R.Battiston,[35] A.Bay,[23] F.Becattini,[17] U.Becker,[16] F.Behner,[50] J.Berdugo,[27] P.Berges,[16] B.Bertucci,[18] B.L.Betev,[50] M.Biasini,[18] A.Biland,[50] G.M.Bilei[35] J.J.Blaising,[18] S.C.Blyth,[36] G.J.Bobbink,[2] R.Bock,[1] A.Böhm,[1] B.Borgia,[38] A.Boucham,[4] D.Bourilkov,[50] M.Bourquin,[20] D.Boutigny,[4] E.Brambilla,[16] J.G.Branson,[41] V.Brigljevic,[50] I.C.Brock,[36] A.Buijs,[46] A.Bujak,[47] J.D.Burger,[16] W.J.Burger,[20] J.Busenitz,[45] A.Buytenhuijs,[32] X.D.Cai,[19] M.Campanelli,[50] M.Capell,[16] G.Cara Romeo,[9] M.Caria,[35] G.Carlino,[4] A.M.Cartacci,[17] J.Casaus,[27] G.Castellini,[17] R.Castello,[28] F.Cavallari,[38] N.Cavallo,[30] C.Cecchi,[20] M.Cerrada,[27] F.Cesaroni,[24] M.Chamizo,[27] A.Chan,[52] Y.H.Chang,[52] U.K.Chaturvedi,[19] M.Chemarin,[26] A.Chen,[52] G.Chen,[7] G.M.Chen,[7] H.F.Chen,[21] H.S.Chen,[7] M.Chen,[16] G.Chiefari,[30] C.Y.Chien,[5] M.T.Choi,[44] L.Cifarelli,[40] F.Cindolo,[9] C.Civinini,[17] I.Clare,[16] R.Clare,[16] H.O.Cohn,[33] G.Coignet,[4] A.P.Colijn,[2] N.Colino,[27] S.Costantini,[38] F.Cotorobai,[13] B.de la Cruz,[27] A.Csilling,[14] T.S.Dai,[16] R.D'Alessandro,[17] R.de Asmundis,[30] H.De Boeck,[32] A.Degré,[4] K.Deiters,[48] P.Denes,[37] F.DeNotaristefani,[38] D.DiBitonto,[45] M.Diemoz,[38] D.van Dierendonck,[2] F.Di Lodovico,[50] C.Dionisi,[38] M.Dittmar,[50] A.Dominguez,[41] A.Doria,[30] I.Dorne,[4] M.T.Dova,[19,♯] E.Drago,[30] D.Duchesneau,[4] P.Duinker,[2] I.Duran,[42] S.Dutta,[10] S.Easo,[35] Yu.Efremenko,[33] H.El Mamouni,[26] A.Engler,[36] F.J.Eppling,[16] F.C.Erné,[2] J.P.Ernenwein,[26] P.Extermann,[20] M.Fabre,[48] R.Faccini,[38] S.Falciano,[38] A.Favara,[17] J.Fay,[26] M.Felcini,[50] C.Furetta,[28] T.Ferguson,[36] D.Fernandez,[27] F.Ferroni,[38] H.Fesefeldt,[1] E.Fiandrini,[35] J.H.Field,[20] F.Filthaut,[36] P.H.Fisher,[16] G.Forconi,[16] L.Fredj,[20] K.Freudenreich,[50] Yu.Galaktionov,[29,16] S.N.Ganguli,[10] S.S.Gau,[12] S.Gentile,[38] J.Gerald,[5] N.Gheordanescu,[13] S.Giagu,[38] S.Goldfarb,[23] J.Goldstein,[11] Z.F.Gong,[21] A.Gougas,[5] G.Gratta,[34] M.W.Gruenewald,[8] V.K.Gupta,[37] A.Gurtu,[10] L.J.Gutay,[47] K.Hangarter,[1] B.Hartmann,[1] A.Hasan,[31] T.Hebbeker,[8] A.Hervé,[18] W.C.van Hoek,[32] H.Hofer,[50] H.Hoorani,[20] S.R.Hou,[52] G.Hu,[19] M.M.Ilyas,[19] V.Innocente,[18] H.Janssen,[4] B.N.Jin,[7] L.W.Jones,[3] P.de Jong,[16] I.Josa-Mutuberria,[27] A.Kasser,[23] R.A.Khan,[19] Yu.Kamyshkov,[33] P.Kapinos,[49] J.S.Kapustinsky,[25] Y.Karyotakis,[4] M.Kaur,[19,◇] M.N.Kienzle-Focacci,[20] D.Kim,[5] J.K.Kim,[44] S.C.Kim,[44] Y.G.Kim,[44] W.W.Kinnison,[25] A.Kirkby,[34] D.Kirkby,[34] J.Kirkby,[18] D.Kiss,[14] W.Kittel,[32] A.Klimentov,[16,29] A.C.König,[32] I.Korolko,[29] V.Koutsenko,[16,29] A.Koulbardis,[39] R.W.Kraemer,[36] T.Kramer,[16] W.Krenz,[1] H.Kuijten,[32] A.Kunin,[16,29] P.Ladron de Guevara,[27] G.Landi,[17] C.Lapoint,[16] K.Lassila-Perini,[50] P.Laurikainen,[22] M.Lebeau,[18] A.Lebedev,[16] P.Lebrun,[26] P.Lecomte,[50] P.Lecoq,[18] P.Le Coultre,[50] J.S.Lee,[44] K.Y.Lee,[44] C.Leggett,[3] J.M.Le Goff,[18] R.Leiste,[49] M.Lenti,[17] E.Leonardi,[38] P.Levtchenko,[39] C.Li,[21] E.Lieb,[49] W.T.Lin,[52] F.L.Linde,[2,18] L.Lista,[30] Z.A.Liu,[7] W.Lohmann,[49] E.Longo,[38] W.Lu,[34] Y.S.Lu,[7] K.Lübelsmeyer,[1] C.Luci,[38] D.Luckey,[16] L.Ludovici,[38] L.Luminari,[38] W.Lustermann,[48] W.G.Ma,[21] A.Macchiolo,[17] M.Maity,[10] G.Majumder,[10] L.Malgeri,[38] A.Malinin,[29] C.Maña,[27] S.Mangla,[10] P.Marchesini,[50] A.Marin,[11] J.P.Martin,[26] F.Marzano,[38] G.G.G.Massaro,[2] K.Mazumdar,[10] D.McNally,[18] S.Mele,[30] L.Merola,[30] M.Meschini,[17] W.J.Metzger,[32] M.von der Mey,[1] Y.Mi,[23] A.Mihul,[13] A.J.W.van Mil,[32] G.Mirabelli,[38] J.Mnich,[18] B.Monteleoni,[17] R.Moore,[3] S.Morganti,[38] R.Mount,[34] S.Müller,[1] F.Muheim,[20] E.Nagy,[14] S.Nahn,[16] M.Napolitano,[30] F.Nessi-Tedaldi,[50] H.Newman,[34] A.Nippe,[1] H.Nowak,[49] G.Organtini,[38] R.Ostonen,[22] D.Pandoulas,[1] S.Paoletti,[38] P.Paolucci,[30] H.K.Park,[36] G.Pascale,[38] G.Passaleva,[17] S.Patricelli,[30] T.Paul,[12] M.Pauluzzi,[35] C.Paus,[1] F.Pauss,[50] D.Peach,[18] Y.J.Pei,[1] S.Pensotti,[28] D.Perret-Gallix,[4] S.Petrak,[8] A.Pevsner,[5] D.Piccolo,[30] M.Pieri,[17] J.C.Pinto,[36] P.A.Piroué,[37] E.Pistolesi,[17] V.Plyaskin,[29] M.Pohl,[50] V.Pojidaev,[29,17] H.Postema,[16] N.Produit,[20] R.Raghavan,[10] G.Rahal-Callot,[50] P.G.Rancoita,[28] M.Rattaggi,[28] G.Raven,[41] P.Razis,[31] K.Read,[33] D.Ren,[50] M.Rescigno,[38] S.Reucroft,[12] T.van Rhee,[46] S.Riemann,[49] B.C.Riemers,[47] K.Riles,[3] O.Rind,[3] S.Ro,[44] A.Robohm,[50] J.Rodin,[16] F.J.Rodriguez,[27] B.P.Roe,[3] S.Röhner,[1] L.Romero,[27] S.Rosier-Lees,[4] Ph.Rosselet,[23] W.van Rossum,[46] S.Roth,[1] J.A.Rubio,[18] H.Rykaczewski,[50] J.Salicio,[18] E.Sanchez,[27] A.Santocchia,[35] M.E.Sarakinos,[22] S.Sarkar,[10] M.Sassowsky,[1] G.Sauvage,[4] C.Schäfer,[1] V.Schegelsky,[39] S.Schmidt-Kaerst,[1] D.Schmitz,[1] P.Schmitz,[1] M.Schneegans,[4] B.Schoeneich,[49] N.Scholz,[50] H.Schopper,[51] D.J.Schotanus,[32] J.Schwenke,[1] G.Schwering,[1] C.Sciacca,[30] D.Sciarrino,[20] J.C.Sens,[52] L.Servoli,[35] S.Shevchenko,[34] N.Shivarov,[43] V.Shoutko,[29] J.Shukla,[25] E.Shumilov,[29] T.Siedenburg,[1] D.Son,[44] A.Sopczak,[49] V.Soulimov,[30] B.Smith,[16] P.Spillantini,[17] M.Steuer,[16] D.P.Stickland,[37] F.Sticozzi,[16] H.Stone,[37] B.Stoyanov,[43] A.Straessner,[1] K.Strauch,[15] K.Sudhakar,[10] G.Sultanov,[19] L.Z.Sun,[21] G.F.Susinno,[20] H.Suter,[50] J.D.Swain,[19] X.W.Tang,[7] L.Tauscher,[6] L.Taylor,[12] Samuel C.C.Ting,[16] S.M.Ting,[16] F.Tonisch,[49] M.Tonutti,[1] S.C.Tonwar,[10] J.Tóth,[14] A.Tsaregorodtsev,[39] C.Tully,[37] H.Tuchscherer,[45] K.L.Tung,[7] J.Ulbricht,[50] U.Uwer,[18] E.Valente,[38] R.T.Van de Walle,[32] G.Vesztergombi,[14] I.Vetlitsky,[29] G.Viertel,[50] M.Vivargent,[4] R.Völkert,[49] H.Vogel,[36] H.Vogt,[49] I.Vorobiev,[29] A.A.Vorobyov,[39] An.A.Vorobyov,[39] A.Vorvolakos,[31] M.Wadhwa,[6] W.Wallraff,[1] J.C.Wang,[16] X.L.Wang,[21] Y.F.Wang,[16] Z.M.Wang,[21] A.Weber,[1] F.Wittgenstein,[18] S.X.Wu,[19] S.Wynhoff,[1] J.Xu,[11] Z.Z.Xu,[21] B.Z.Yang,[21] C.G.Yang,[7] X.Y.Yao,[7] J.B.Ye,[21] S.C.Yeh,[52] J.M.You,[36] C.Zaccardelli,[34] An.Zalite,[39] P.Zemp,[50] Y.Zeng,[1] Z.Zhang,[7] Z.P.Zhang,[21] B.Zhou,[11] Y.Zhou,[3] G.Y.Zhu,[7] R.Y.Zhu,[34] A.Zichichi.[9,18,19]

1 I. Physikalisches Institut, RWTH, D-52056 Aachen, FRG[§]
III. Physikalisches Institut, RWTH, D-52056 Aachen, FRG[§]
2 National Institute for High Energy Physics, NIKHEF, and University of Amsterdam, NL-1009 DB Amsterdam, The Netherlands
3 University of Michigan, Ann Arbor, MI 48109, USA
4 Laboratoire d'Annecy-le-Vieux de Physique des Particules, LAPP,IN2P3-CNRS, BP 110, F-74941 Annecy-le-Vieux CEDEX, France
5 Johns Hopkins University, Baltimore, MD 21218, USA
6 Institute of Physics, University of Basel, CH-4056 Basel, Switzerland
7 Institute of High Energy Physics, IHEP, 100039 Beijing, China
8 Humboldt University, D-10099 Berlin, FRG[§]
9 INFN-Sezione di Bologna, I-40126 Bologna, Italy
10 Tata Institute of Fundamental Research, Bombay 400 005, India
11 Boston University, Boston, MA 02215, USA
12 Northeastern University, Boston, MA 02115, USA
13 Institute of Atomic Physics and University of Bucharest, R-76900 Bucharest, Romania
14 Central Research Institute for Physics of the Hungarian Academy of Sciences, H-1525 Budapest 114, Hungary[‡]
15 Harvard University, Cambridge, MA 02139, USA
16 Massachusetts Institute of Technology, Cambridge, MA 02139, USA
17 INFN Sezione di Firenze and University of Florence, I-50125 Florence, Italy
18 European Laboratory for Particle Physics, CERN, CH-1211 Geneva 23, Switzerland
19 World Laboratory, FBLJA Project, CH-1211 Geneva 23, Switzerland
20 University of Geneva, CH-1211 Geneva 4, Switzerland
21 Chinese University of Science and Technology, USTC, Hefei, Anhui 230 029, China
22 SEFT, Research Institute for High Energy Physics, P.O. Box 9, SF-00014 Helsinki, Finland
23 University of Lausanne, CH-1015 Lausanne, Switzerland
24 INFN-Sezione di Lecce and Universitá Degli Studi di Lecce, I-73100 Lecce, Italy
25 Los Alamos National Laboratory, Los Alamos, NM 87544, USA
26 Institut de Physique Nucléaire de Lyon, IN2P3-CNRS,Université Claude Bernard, F-69622 Villeurbanne, France
27 Centro de Investigaciones Energeticas, Medioambientales y Tecnologicas, CIEMAT, E-28040 Madrid, Spain[♭]
28 INFN-Sezione di Milano, I-20133 Milan, Italy
29 Institute of Theoretical and Experimental Physics, ITEP, Moscow, Russia
30 INFN-Sezione di Napoli and University of Naples, I-80125 Naples, Italy
31 Department of Natural Sciences, University of Cyprus, Nicosia, Cyprus
32 University of Nymegen and NIKHEF, NL-6525 ED Nymegen, The Netherlands
33 Oak Ridge National Laboratory, Oak Ridge, TN 37831, USA
34 California Institute of Technology, Pasadena, CA 91125, USA
35 INFN-Sezione di Perugia and Universitá Degli Studi di Perugia, I-06100 Perugia, Italy
36 Carnegie Mellon University, Pittsburgh, PA 15213, USA
37 Princeton University, Princeton, NJ 08544, USA
38 INFN-Sezione di Roma and University of Rome, "La Sapienza", I-00185 Rome, Italy
39 Nuclear Physics Institute, St. Petersburg, Russia
40 University and INFN, Salerno, I-84100 Salerno, Italy
41 University of California, San Diego, CA 92093, USA
42 Dept. de Fisica de Particulas Elementales, Univ. de Santiago, E-15706 Santiago de Compostela, Spain
43 Bulgarian Academy of Sciences, Central Laboratory of Mechatronics and Instrumentation, BU-1113 Sofia, Bulgaria
44 Center for High Energy Physics, Korea Advanced Inst. of Sciences and Technology, 305-701 Taejon, Republic of Korea
45 University of Alabama, Tuscaloosa, AL 35486, USA
46 Utrecht University and NIKHEF, NL-3584 CB Utrecht, The Netherlands
47 Purdue University, West Lafayette, IN 47907, USA
48 Paul Scherrer Institut, PSI, CH-5232 Villigen, Switzerland
49 DESY-Institut für Hochenergiephysik, D-15738 Zeuthen, FRG
50 Eidgenössische Technische Hochschule, ETH Zürich, CH-8093 Zürich, Switzerland
51 University of Hamburg, D-22761 Hamburg, FRG
52 High Energy Physics Group, Taiwan, China
§ Supported by the German Bundesministerium für Bildung, Wissenschaft, Forschung und Technologie
‡ Supported by the Hungarian OTKA fund under contract number T14459.
♭ Supported also by the Comisión Interministerial de Ciencia y Technología
♯ Also supported by CONICET and Universidad Nacional de La Plata, CC 67, 1900 La Plata, Argentina
◇ Also supported by Panjab University, Chandigarh-160014, India

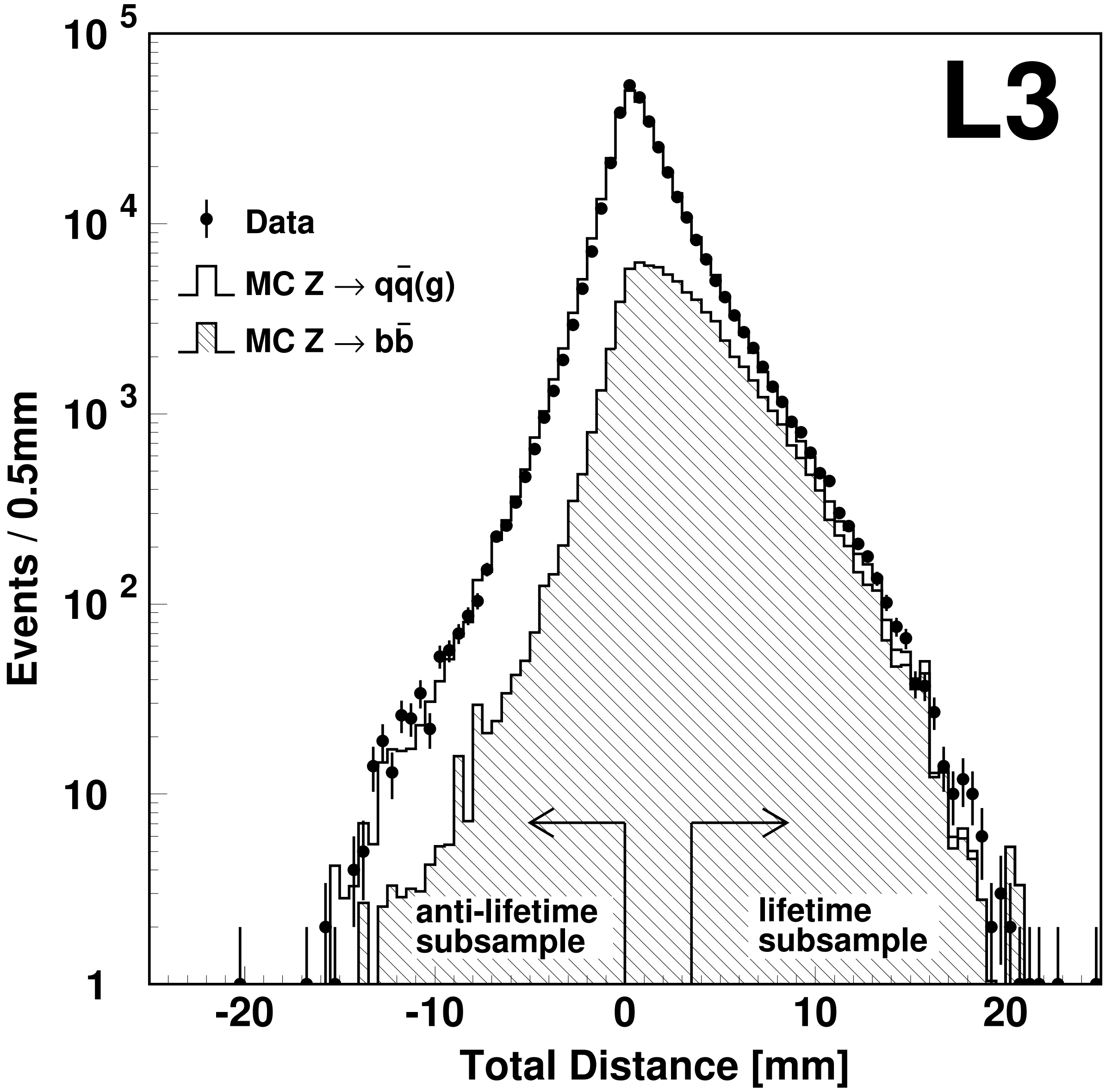

Figure 1: Distribution of the measured distance between the two reconstructed jet vertices in the data and in Monte Carlo simulated hadronic Z decays. The fraction of b events in the Monte Carlo is also shown. The lifetime subsample (I) and anti–lifetime subsample (II) are the events with a reconstructed distance of more than 3.5 mm or less than 0.0 mm respectively.

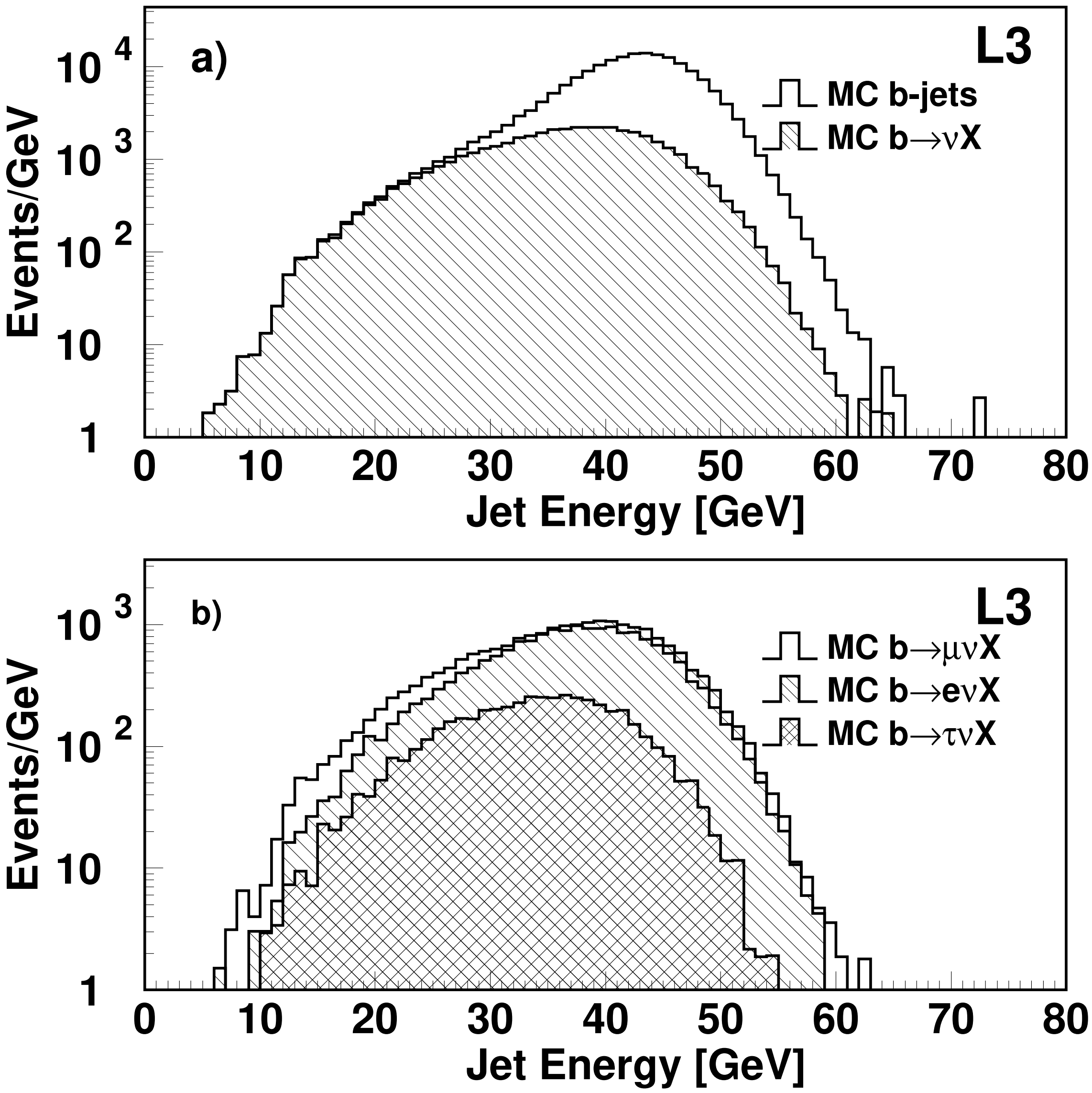

Figure 2: (a) The visible energy spectrum of jets in the Monte Carlo from the b jets together with the contributions from semileptonic b hadron decays and (b) the visible jet energy spectrum for the different types of semileptonic b hadron decays.

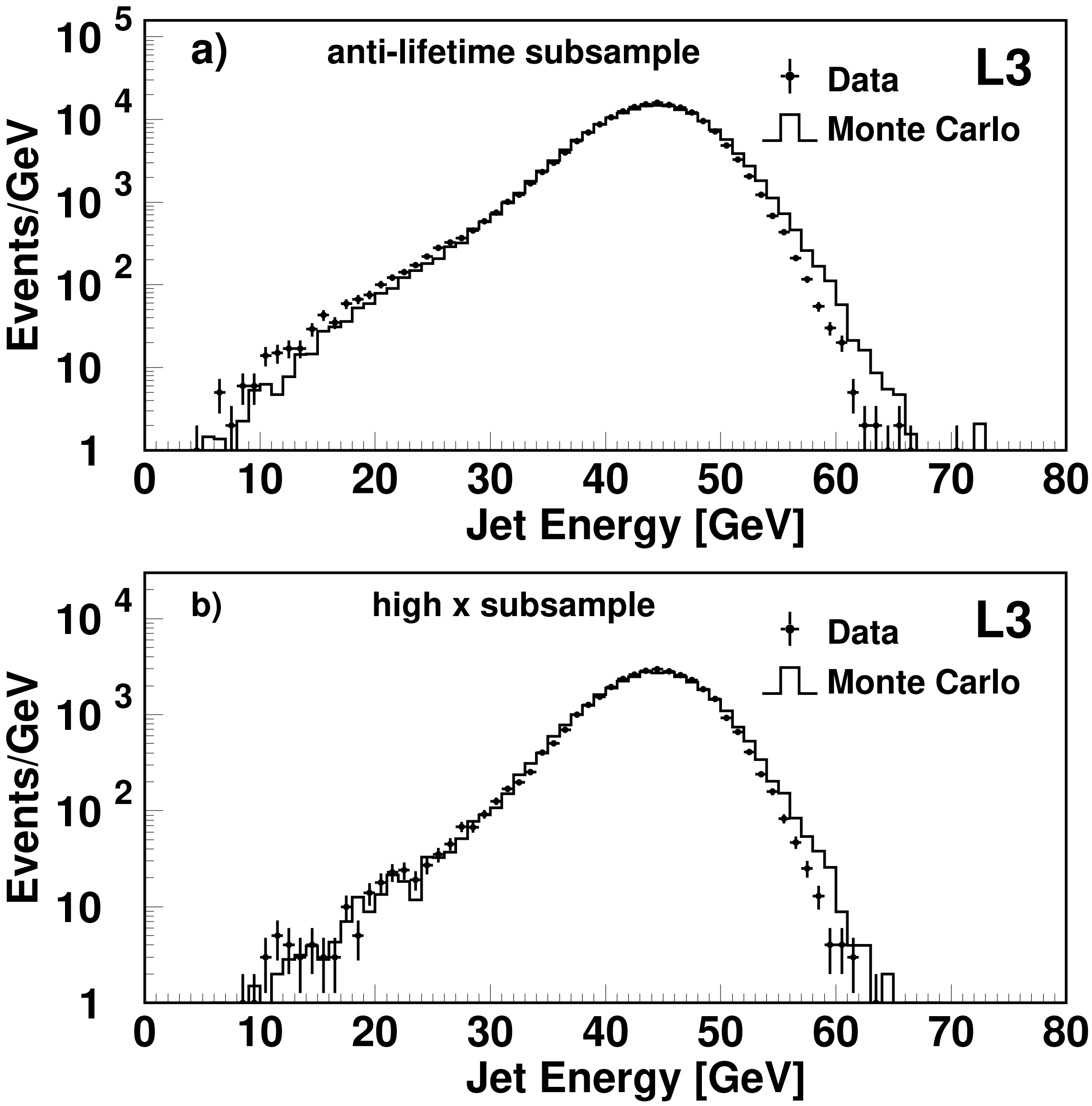

Figure 3: The visible energy spectrum of b depleted jets in the data and in the Monte Carlo.

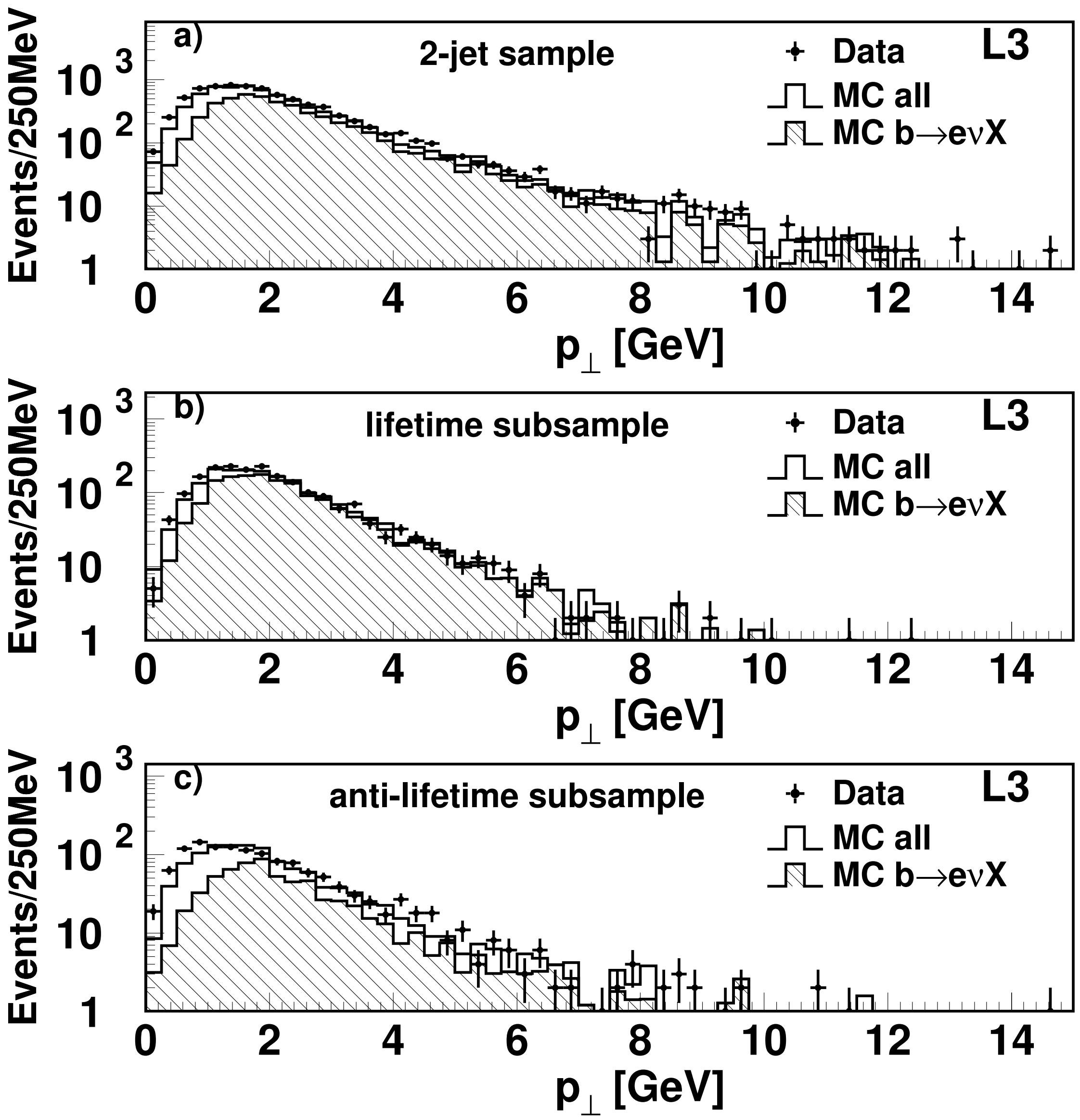

Figure 4: (a) The $p_\perp$ spectrum with respect to the jet direction for the electron candidates in the two–jet sample, (b) in the b enriched subsample I and (c) in the b depleted subsample II. The corresponding Monte Carlo distributions are also shown, together with the fraction of correctly identified semileptonic b decays using a branching ratio of 10.45%.

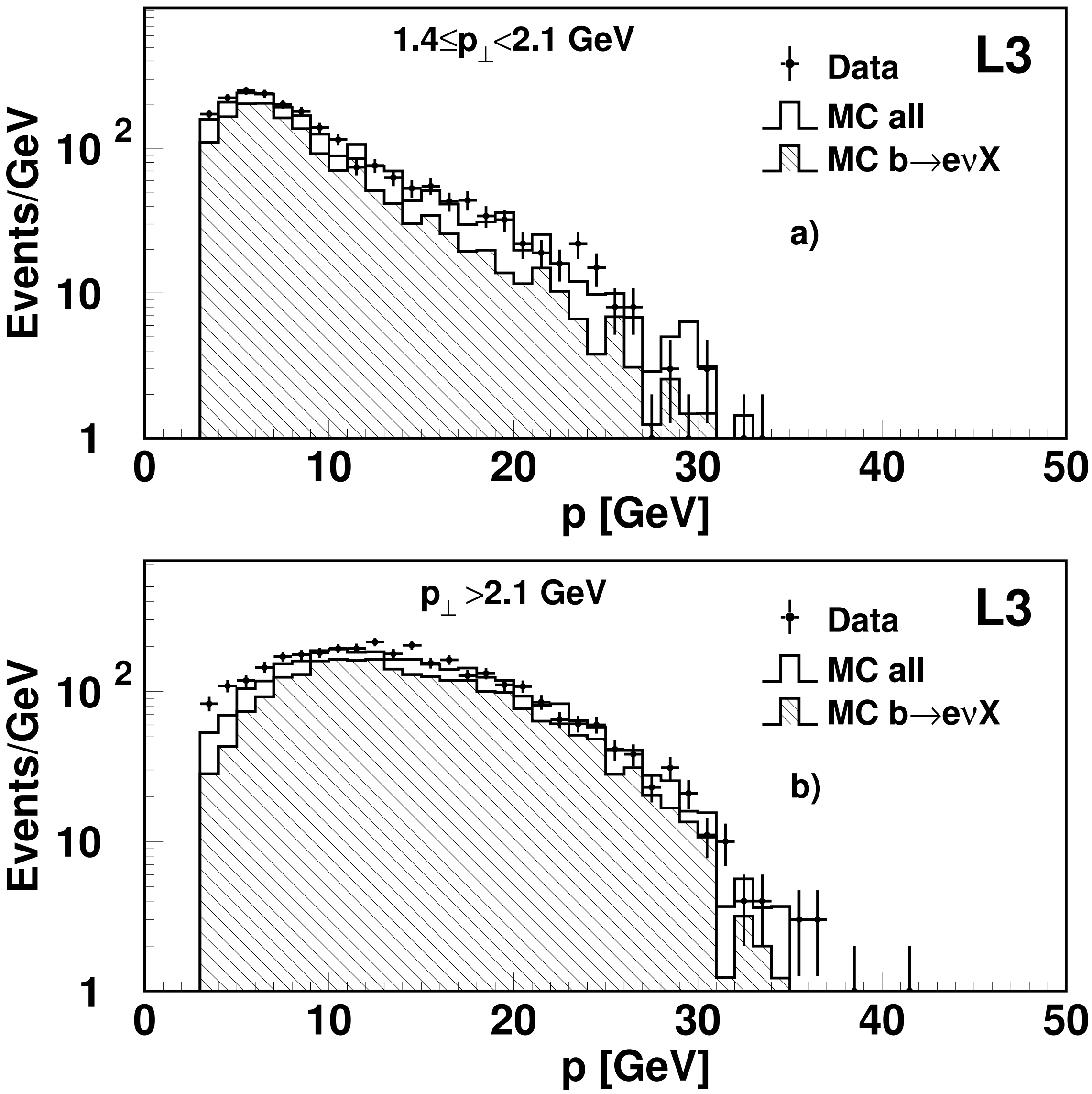

Figure 5: (a) The momentum spectrum of the electron candidates with a $p_\perp$ with respect to the jet direction between 1.4–2.1 GeV and (b) for $p_\perp$ values of more than 2.1 GeV. The corresponding Monte Carlo distributions are also shown, together with the fraction of correctly identified semileptonic b decays using a branching ratio of 10.45%.

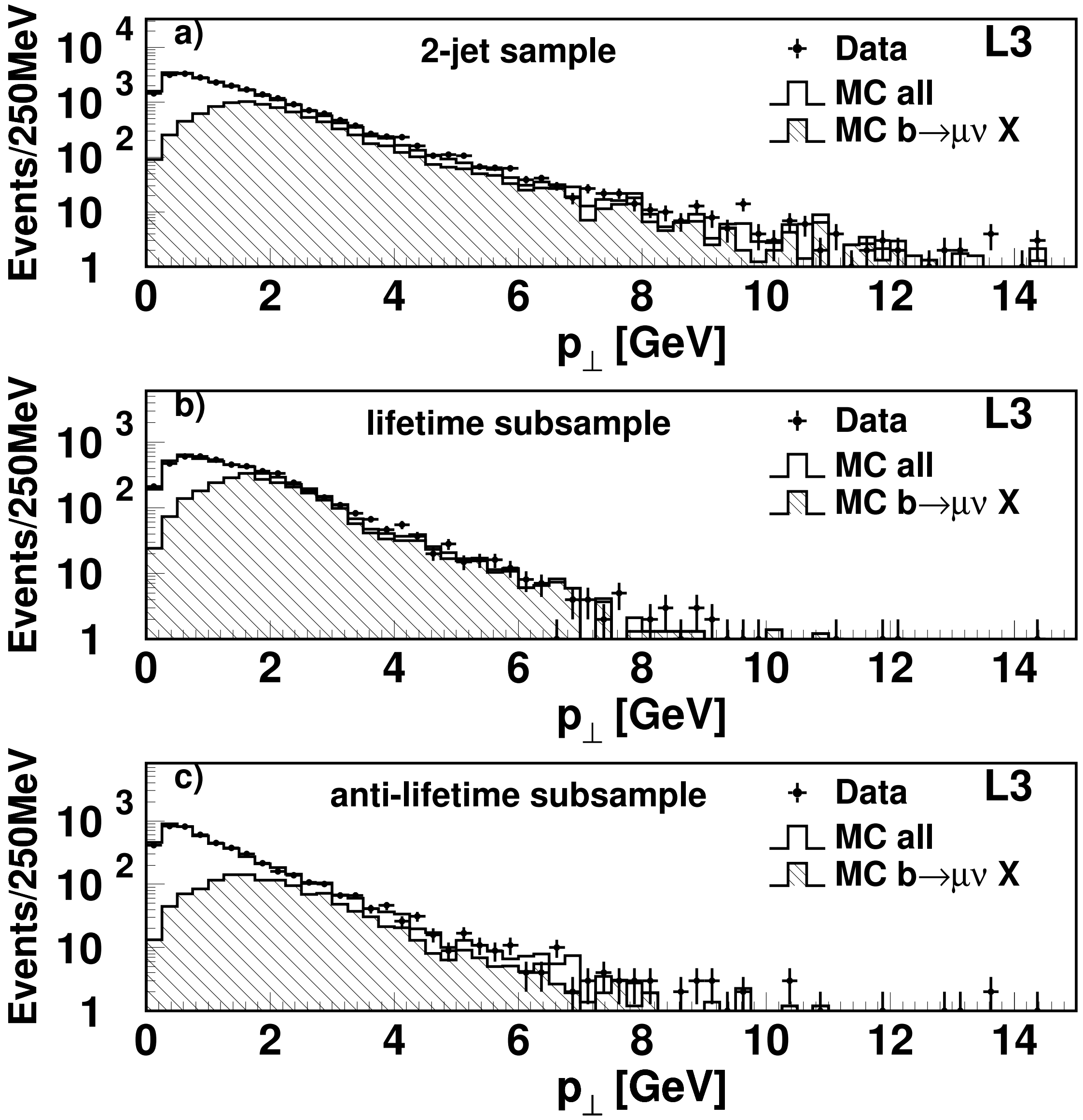

Figure 6: (a) The $p_\perp$ spectrum with respect to the jet direction for the muon candidates in the two–jet sample, (b) in the b enriched subsample I and (c) in the b depleted sample II. The corresponding Monte Carlo distributions are also shown, together with the fraction of correctly identified semileptonic b decays using a branching ratio of 10.45%.

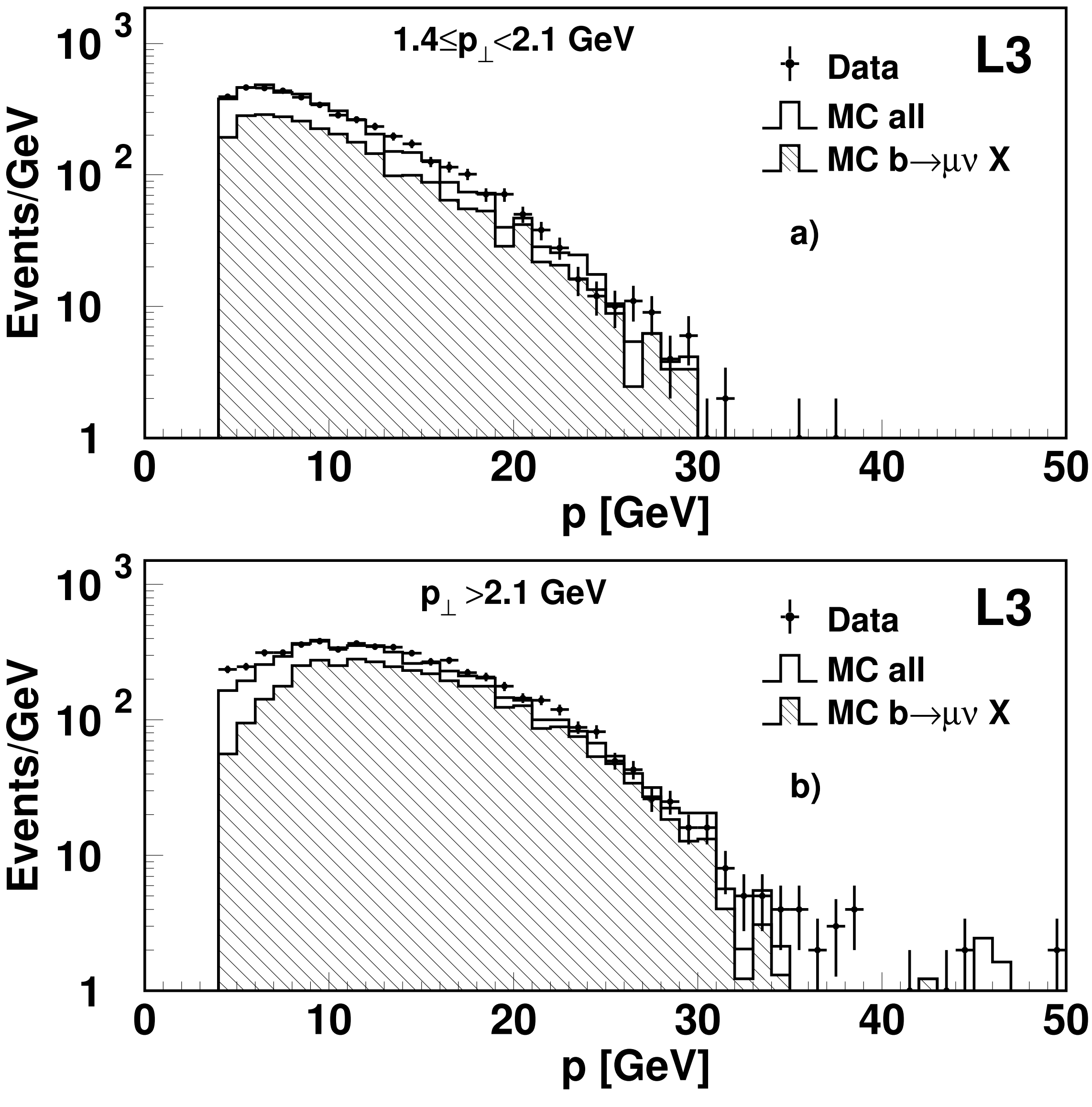

Figure 7: (a) The p spectrum of the muon candidates with a $p_\perp$ with respect to the jet direction between 1.4–2.1 GeV and (b) for $p_\perp$ values of more than 2.1 GeV. The corresponding Monte Carlo distributions are also shown, together with the fraction of correctly identified semileptonic b decays using a branching ratio of 10.45%.

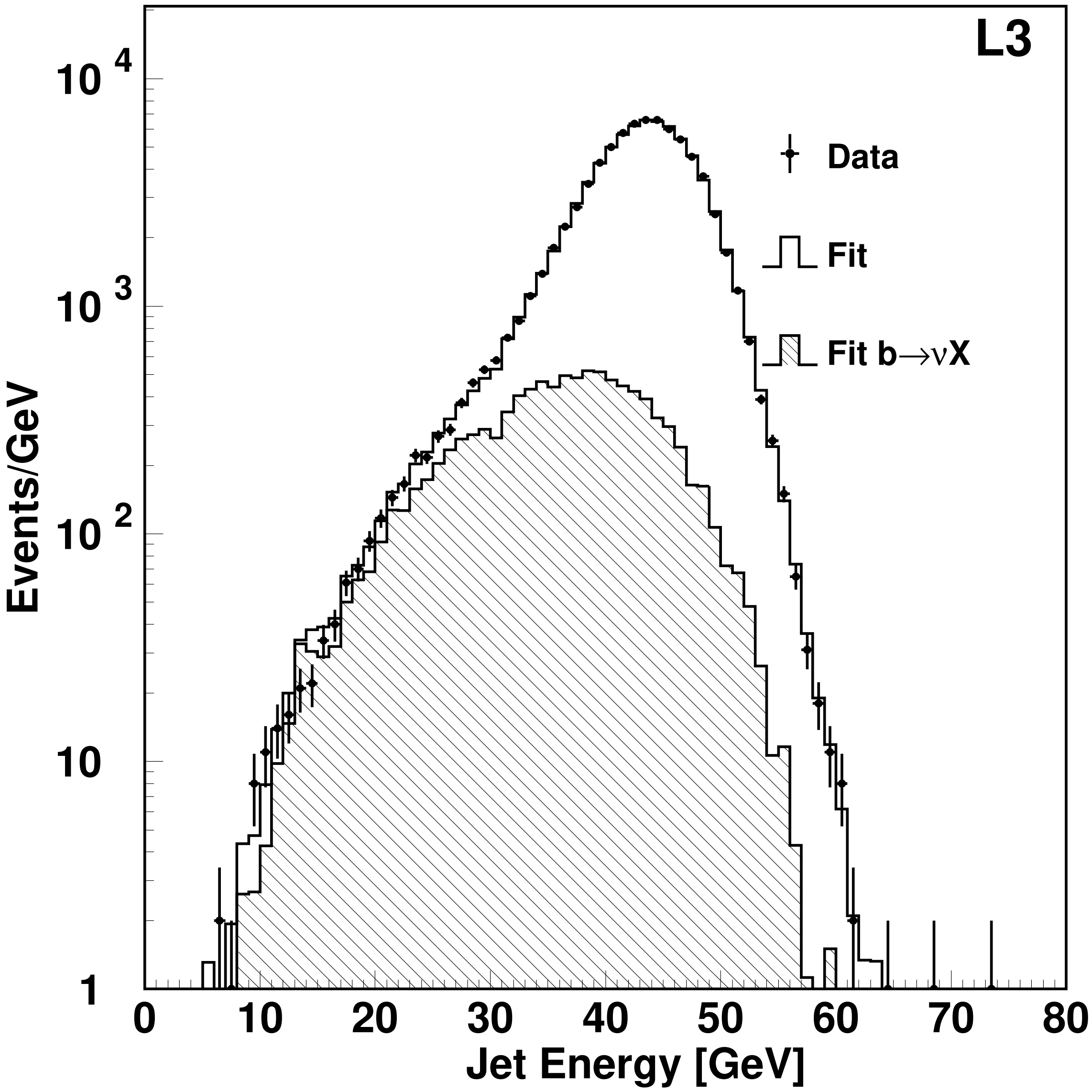

Figure 8: The jet energy spectrum from subsample I in the data and the results of the fit for the measurement of Br(b→ νX).

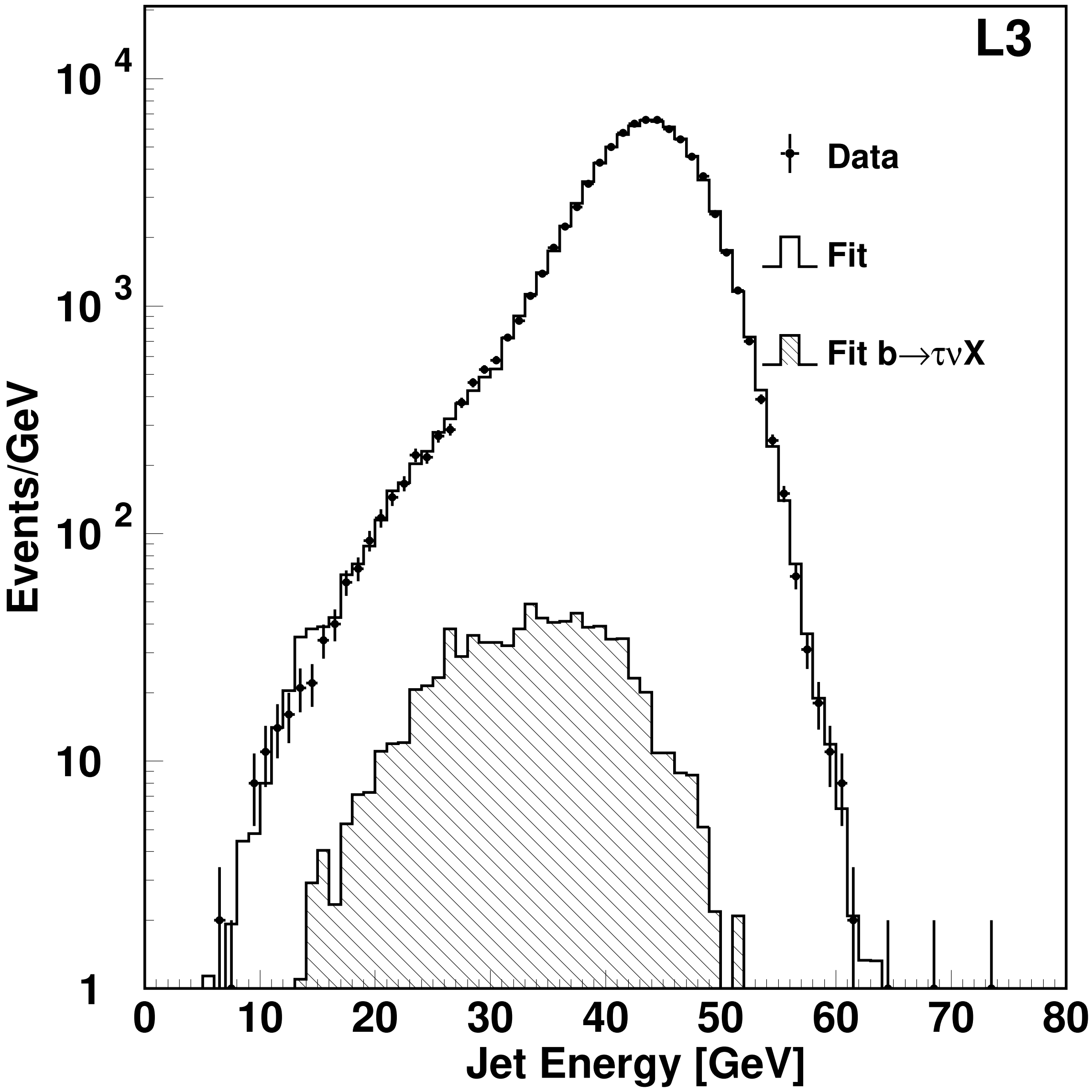

Figure 9: The jet energy spectrum of subsample I in the data and the results of the fit for the measurement of Br(b$\rightarrow \tau\nu$X) with the constrain Br(b$\rightarrow$ e(μ)νX)=10.85%.

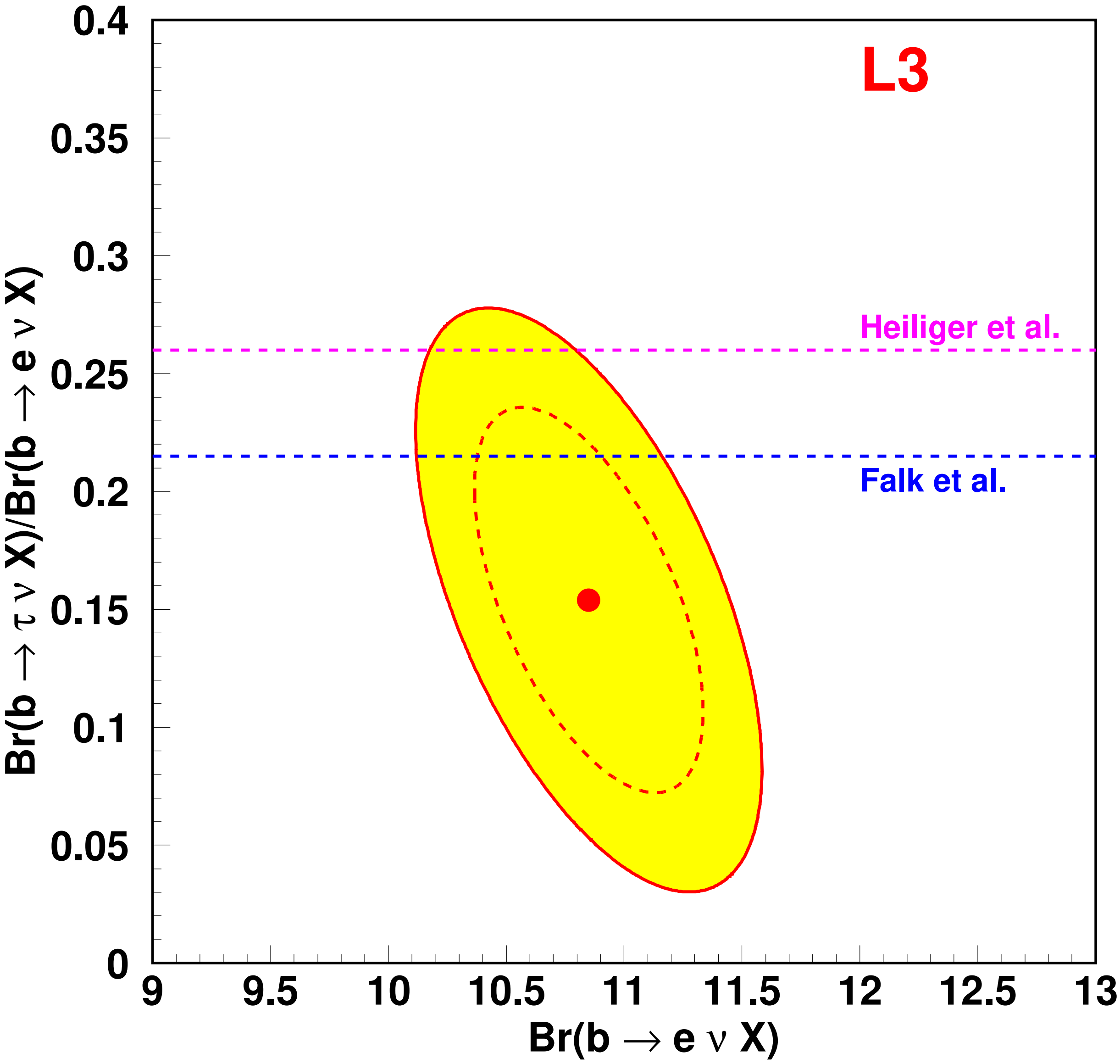

Figure 10: Comparison of theoretical predictions [15] with the measurement for the ratio Br(b→ $\tau\nu$X)/Br(b→ $e\nu$X) as a function of the of Br(b→ $e\nu$X). Shown are the 39% (dashed ellipse) and 68% (solid ellipse) confidence level contours.